MPMI Vol. 25, No. 5, 2012, pp. 709–723. http://dx.doi.org/10.1094/MPMI-11-11-0305. © 2012 The American Phytopathological Society *e*-Xtra*

Comparative Analysis of Transcriptomic and Hormonal Responses to Compatible and Incompatible Plant-Virus Interactions that Lead to Cell Death

Remedios Pacheco,[1] Alberto García-Marcos,[1] Aranzazu Manzano,[1] Mario García de Lacoba,[1] Gemma Camañes,[2] Pilar García-Agustín,[2] José Ramón Díaz-Ruíz,[1] and Francisco Tenllado[1]

[1]Departamento de Biología Medioambiental, Centro de Investigaciones Biológicas, CSIC, Ramiro de Maeztu 9, 28040, Madrid, Spain; [2]Grupo de Bioquímica y Biotecnología. Área de Fisiología Vegetal, Departamento de Ciencias Agrarias y del Medio Natural, ESTCE, Universitat Jaume I, 12071, Castellón, Spain

Submitted 30 November 2011. Accepted 9 January 2012.

Hypersensitive response-related programmed cell death (PCD) has been extensively analyzed in various plant–virus interactions. However, little is known about the changes in gene expression and phytohormone levels associated with cell death caused by compatible viruses. The synergistic interaction of *Potato virus X* (PVX) with a number of *Potyvirus* spp. results in increased symptoms that lead to systemic necrosis (SN) in *Nicotiana benthamiana.* Here, we show that SN induced by a PVX recombinant virus expressing a potyviral helper component-proteinase (HC-Pro) gene is associated with PCD. We have also compared transcriptomic and hormonal changes that occur in response to a compatible synergistic virus interaction that leads to SN, a systemic incompatible interaction conferred by the *Tobacco mosaic virus*-resistance gene *N*, and a PCD response conditioned by depletion of proteasome function. Our analysis indicates that the SN response clusters with the incompatible response by the similarity of their overall gene expression profiles. However, the expression profiles of both defense-related genes and hormone-responsive genes, and also the relative accumulation of several hormones in response to SN, relate more closely to the response to depletion of proteasome function than to that elicited by the incompatible interaction. This suggests a potential contribution of proteasome dysfunction to the increased pathogenicity observed in PVX–*Potyvirus* mixed infections. Furthermore, silencing of *coronatine insensitive 1*, a gene involved in jasmonate perception, in *N. benthamiana* accelerated cell death induced by PVX expressing HC-Pro.

Virus infections are the cause of numerous plant disease syndromes in susceptible hosts. One of the most severe symptoms elicited by many plant viruses is systemic necrosis (SN), which causes not only developmental arrest but also leaf or plant death over the course of several days. The molecular mechanisms of SN induction in susceptible hosts seem different from the so-called hypersensitive response (HR) that is induced within hours in response to incompatible virus–host interactions. HR, a form of programmed cell death (PCD) (Dangl and Jones 2001), is initiated at infection sites and limits virus spread in association with localized death of infected and neighboring cells, inducing a variety of defense-related genes and a wide range of physiological changes, which usually involve direct or indirect recognition between avirulence (*Avr*) factors and host resistance (*R*) genes (Hammond-Kosack and Jones 1996).

Several lines of evidence have shown that SN shares HR attributes, such as the induction of PCD, the expression of defense-related genes, and the production of reactive oxygen species (ROS) (García-Marcos et al. 2009; Kim et al. 2008; Komatsu et al. 2010; Lamb et al. 1997; Xu and Roossinck 2000). Moreover, several studies have suggested that SN may result from a gene-for-gene interaction, in some cases through *R* gene recognition (Atsumi et al. 2009; Kim et al. 2010; Király et al. 1999). In addition, perturbation of *Avr–R* recognition during incompatible interactions occasionally results in virus escape to distant tissues provoking systemic HR (SHR), a phenotype that resembles SN (Dinesh-Kumar et al. 2000; Seo et al. 2006). Whether the host utilizes the same molecular or cellular circuits in processing cell death signals induced by both compatible and incompatible interactions is not known.

Significant progress has been made in characterizing incompatible plant–virus interactions that induce PCD and disease resistance (Lewsey et al. 2009). However, very little is known about how compatible viruses induce PCD-like processes, although several studies have identified viral symptom determinants responsible for SN (Burgyan et al. 2000; Király et al. 1999; Komatsu et al. 2011). Because both types of necrosis responses share molecular and biochemical features, a comparative study could shed light on their similarities and differences. In particular, the magnitude and complexity of gene expression changes that occur during a compatible plant–virus interaction that leads to SN have never been compared at the genome level with those induced by an incompatible interaction. Additionally, although several phytohormones are known to act as signal molecules in defense responses (Kunkel and Brooks 2002), a comprehensive study of their involvement in SN has not been undertaken.

The National Center for Biotechnology Information Gene Expression Omnibus accession number for the microarray data from this work is GSE34841.

Corresponding author: F. Tenllado; Telephone: +34-1-8373112; Fax: +34-1-5360432; E-mail: tenllado@cib.csic.es

*The *e*-Xtra logo stands for "electronic extra" and indicates that five supplementary figures and three supplementary tables are published online and that Figures 1, 2, 3, 4, 5, and 7 appear in color online.

Compared with single infections, co-infection of *Nicotiana benthamiana* with *Potato virus X* (PVX) and *Potato virus Y* (PVY) resulted in increased systemic symptoms (synergism) that led to SN in the newly emerging leaves, and to plant death. Accordingly, it induced a severe oxidative stress in plant leaves, as judged by increases in lipid peroxidation and by the generation of ROS (García-Marcos et al. 2009). Further, the expression of the potyviral helper component-proteinase (HC-Pro) protein by a PVX vector (PVX/HCWT) was sufficient to induce an increase of PVX pathogenicity that led to SN (González-Jara et al. 2005). *Potyvirus* sp.-associated synergistic diseases have been suggested to result from suppression by the multifunctional HC-Pro of the host defense mechanism based on RNA silencing (Pruss et al. 1997). Moreover, HC-Pro has also been shown to interfere with the microRNA- and small-interfering RNA-mediated regulation of endogenous gene expression (Kasschau et al. 2003). In fact, transgenic expression of PVY HC-Pro alone partially mimicked transcriptional changes previously shown to occur in plants infected with intact viruses, indicating that it is a major factor in viral pathogenicity (Soitamo et al. 2011). However, although overexpression of HC-Pro induced phenotypic changes in both growth rate and morphology of *Nicotiana* spp., the necrosis symptom was never elicited in these transgenic plants. Research on animal viral proteins has revealed that viruses can direct or hijack proteasome function by interacting with the core of the 20S proteasome or with its 19S regulatory particle (Dielen et al. 2010). Evidence that HC-Pro interferes with some of the catalytic activities of the plant 20S proteasome (Ballut et al. 2005; Dielen et al. 2011) suggests the potential contribution of proteasome dysfunction to the increase in pathogenicity observed in PVX–*Potyvirus* infections.

The ubiquitin-proteasome-dependent pathway is involved in the response of plants to most environmental modifications and stresses, including plant–pathogen interactions (Craig et al. 2009; Dielen et al. 2010). Recent advances in hormone signaling research have uncovered a common strategy in which proteasome-mediated degradation complexes are central for the transmission of hormonal signals in plant defense responses (Chini et al. 2009). In addition, the proteasome system also has a major role in the regulation of animal apoptosis, and similar regulatory roles have been postulated for PCD in plants (Hatsugai et al. 2009). It has also been reported that silencing of different subunits of the 20S proteasome by virus-induced gene silencing (VIGS) triggers PCD in plants by inactivating proteasome function (Kim et al. 2003).

In this study, a transcriptome analysis was undertaken in *N. benthamiana* to identify similarities and differences in gene expression profiles between SN induced by a compatible synergistic virus interaction and PCD induced by either an incompatible virus or depletion of proteasome function. Our analysis indicated that, although the SN response was clustered with the incompatible response by the similarity of their overall gene expression profiles, the particular expression profiles of defense-related and hormone-responsive genes in response to SN were more closely related to profiles in response to depletion of proteasome function than to those elicited by the incompatible interaction. Biochemical measurement of salicylic acid (SA), jasmonic acid (JA), and abscissic acid (ABA) levels and expression analysis of marker genes supported these findings, suggesting that SA regulates the differential defense response to the incompatible virus. Furthermore, it was shown that JA signaling mediated through *coronatine insensitive1* (*COI1*) interfered with infection by PVX/HCWT and subsequent cell death in *N. benthamiana*.

RESULTS

Cell death induced by compatible and incompatible viruses, and by depletion of proteasome function.

PVX recombinant virus expressing the *HC-Pro* gene from *Plum pox virus* (PPV) (PVX/HCWT) induced an enhancement of PVX pathogenicity, manifested as necrosis in systemically infected leaves and stems at 11 days postinoculation (dpi), that caused plant death during the course of the following few days (Fig. 1A). A variant of PPV HC-Pro containing a single point mutation ($HCL_{134}H$) was unable to induce this SN response, although plants developed typical PVX symptoms on systemically infected leaves (PVX/HCLH) (González-Jara et al. 2005). Infiltration of plants with *Agrobacterium tumefaciens* harboring a *Tobacco rattle virus* (TRV)-based VIGS vector containing a 520-bp fragment from the *PBE* subunit of the *N. benthamiana* 20S proteasome caused the progression of necrosis from periveinal regions of systemic leaves at 8 days after infiltration (dai), and led to collapse of the plant later on (Kim et al. 2003). Real-time quantitative reverse-transcription polymerase chain reaction (qRT-PCR) analysis showed a markedly reduced accumulation (20-fold) of *NbPBE* transcripts in leaves of *NbPBE*-silenced plants compared with the effect of the empty vector (TRV:00) in control leaves. To examine an incompatible virus–host interaction, we took advantage of the synchronous HR induction system in transgenic *N. benthamiana* plants expressing the *N* gene resistance gene from *N. glutinosa* after infection with a *Tobacco mosaic virus*-based vector expressing free green fluorescent protein (TMV-GFP) (Peart et al. 2002). Shifting TMV-GFP-infected tissues from 30°C, a nonpermissive temperature for HR induction, to 25°C resulted in *Avr–R* recognition that led to a SHR at 72 h after the temperature shift (hts), which was absent in wild-type plants infected with TMV-GFP. Likewise, trypan blue staining revealed the presence of areas of dead cells in wild-type plants infected with PVX/HCWT or TRV:*NbPBE* or in *N* gene-transgenic plants infected with TMV-GFP (Fig. 1B). Such staining was not found in wild-type leaves infected with PVX/HCLH, TRV:00, or TMV-GFP.

Degradation of nuclear DNA is one of the hallmarks of PCD. Therefore, we utilized an assay based on the detection of 3′ hydroxyl groups of degraded nuclear DNA (terminal deoxynucleotidyltransferase-mediated dUTP nick end labeling [TUNEL] assay) (Gavrieli et al. 1992) to investigate whether PCD was involved in the SN induced by PVX/HCWT. We detected cleavage of nuclear DNA in both the mock-inoculated control treated with DNaseI and in plants inoculated with PVX/HCWT (Fig. 1C). Control *N. benthamiana* plants, as well as PVX/HCLH-infected plants, exhibited no detectable staining for nuclear DNA cleavage. No positive signal was noted in sections derived from PVX/HCWT-infected tissues from which the terminal deoxynucleotidyltransferase enzyme was omitted.

Global gene expression comparison.

Six transcriptome comparisons were made in the Agilent's 4-by-44 K Tobacco two-color chip. A design for array hybridizations was used in which labeled aRNA derived from each necrosis-inducing condition was hybridized with labeled aRNA from the corresponding non–necrosis inducing controls. The rationale of this strategy was to discriminate suites of genes that were potentially involved in symptom enhancement (those whose expression was changed significantly) from those that were part of a more general response to virus infection within each comparison. Because the progress of necrosis caused by the pathogens differed among comparisons, two different time points were selected for each comparison, based on early and late stages of infection, as follows: i) PVX/HCWT-infected

plants versus plants infected with PVX/HCLH (hereafter referred to as SN comparison) at 7 and 11 dpi; ii) *NbPBE*-silenced plants versus plants infected with the TRV empty vector (VIGS Prot comparison) at 4 and 8 dai; and iii) TMV-GFP-infected, *N*-transgenic plants versus wild-type plants infected with TMV-GFP (SHR comparison) at 24 and 72 hts. These sampling time points correspond to stages of the infection process prior or subsequent to the emergence of necrotic symptoms in each comparison.

Viral accumulation was measured in the different experimental conditions using virus-specific, qRT-PCR assays on the same pooled RNA extracts used for microarray hybridizations. In general, the magnitude of virus accumulation was higher in plants infected with necrosis-inducing pathogens than in plants infected with non–necrosis inducing pathogens at early and late time points (Fig. 1D). However, PVX/HCLH accumulated to greater levels (twofold) than PVX/HCWT at 7 dpi. By 11 dpi, when cell death was apparent on the upper leaves of PVX/HCWT-infected leaves, accumulation levels of PVX/HCWT were more than five times higher than PVX/HCLH.

Microarray analysis resulted in lists of differentially expressed genes (false discovery rate [FDR] < 0.05) (Supplementary Table S1). Following the dynamics of necrosis appearance, the number of differentially regulated genes was greater at the late time

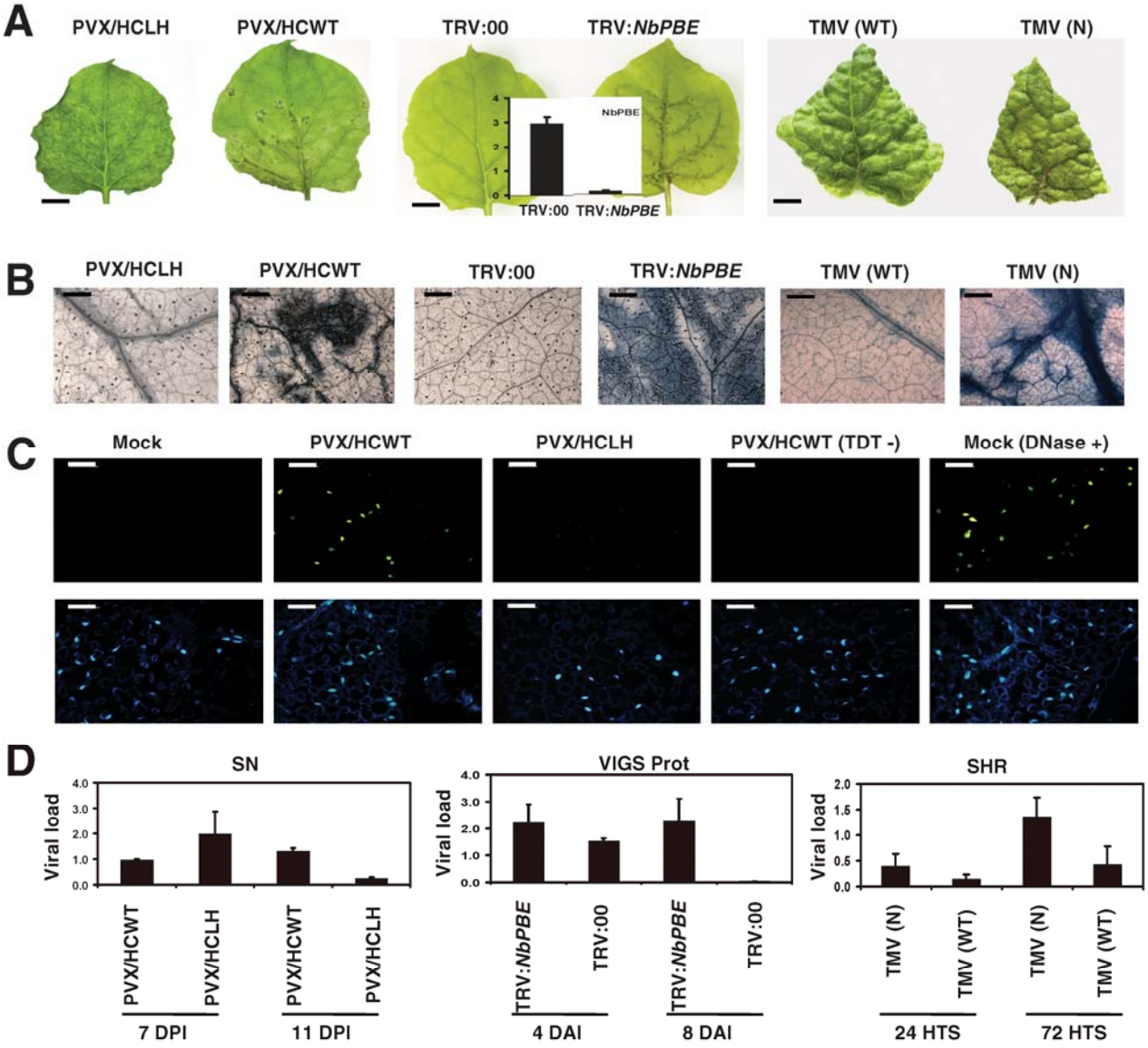

Fig. 1. Cell death induced by three different plant–virus interactions. **A,** Characteristic necrotic symptoms induced by *Potato virus X* (PVX)/HCWT, TRV:*NbPBE*, and *Tobacco mosaic virus*-based vector expressing free green fluorescent protein (TMV-GFP) (*N* plant) in *Nicotiana benthamiana* plants at 11 days postinoculation (dpi), 8 days after infiltration (dai), and 72 h after temperature shift (hts), respectively. Note absence of necrosis in PVX/HCWT-, TRV:00- and TMV-GFP (wild-type [Wt] plant)-infected tissues at the same time points. The relative expression of *NbPBE* in TRV:*NbPBE*-infiltrated plants was estimated by quantitative reverse-transcriptase polymerase chain reaction (qRT-PCR) at 8 dai. Scale bars = 1 cm. **B,** Leaf discs from plants inoculated with the different virus treatments were stained with trypan blue. Detection of cell death areas could be visualized as a dark coloration. Scale bars = 0.5 mm. **C,** Detection of nuclear DNA fragmentation with the transferase-mediated dUTP nick-end labeling (TUNEL) assay (upper panels). Leaf sections from PVX/HCWT-, PVX/HCLH-, and mock-inoculated plants were assayed and observed at 11 dpi. Sections of a mock-inoculated plant were treated with DNase I (DNase +) as a positive control. Sections of a PVX/HCWT-inoculated plant were not treated with the terminal deoxynucleotidyl transferase enzyme (TDT –) as a negative control. Nuclei are indicated by 4′,6-diamidino-2-phenylindole staining (lower panels). Scale bars = 50 µm. **D,** Comparison of relative viral loads estimated by qRT-PCR at early and late stages of infection. RNA samples used for microarray analyses were used to determine the relative levels of PVX/HCWT and PVX/HCLH in systemic necrosis (SN) comparison, TRV:*NbPBE* and TRV:00 in virus-induced gene silencing of proteasome (VIGS Prot) comparison, and TMV-GFP in Wt and *N*-transgenic plants in systemic hypersensitive response (SHR) comparison. Samples were normalized to expression of 18S rRNA transcripts.

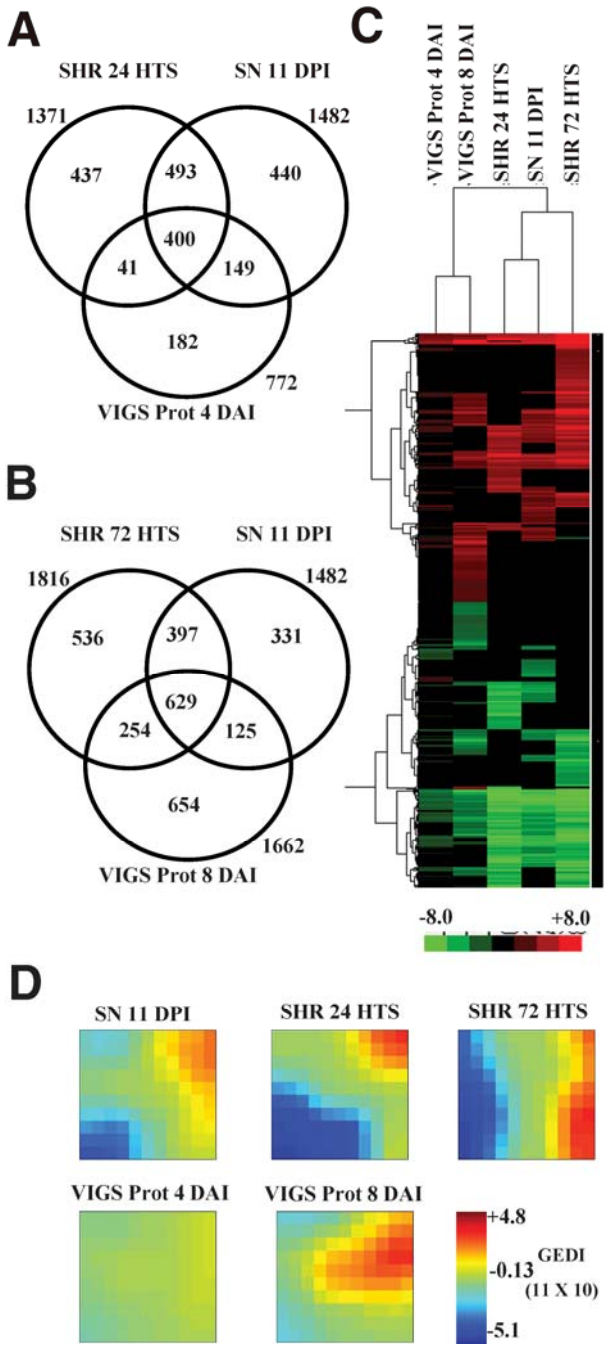

Fig. 2. Number of specific and common differentially expressed genes (DEG), and clustering analysis of DEG in systemic necrosis (SN), systemic hypersensitive response (SHR), and virus-induced gene silencing of proteasome (VIGS Prot) comparisons. Venn diagrams displaying the overlap in DEG between SN at 11 days postinoculation (DPI) and SHR or VIGS Prot at **A,** early (24 h after temperature shift [HTS] and 4 days after infiltration [DAI], respectively) and **B,** late (72 HTS and 8 DAI, respectively) stages of infection. Only genes with changes in expression of 1.5-fold or more (up or down) relative to the controls and a false discovery rate-corrected P value < 0.05 are shown. **C,** Hierarchical cluster analysis of the expression profiles for the 3,258 genes that were differentially expressed in at least one comparison was performed by the Cluster 3.0 program. Expression values are color-coded, with red indicating upregulation, green indicating downregulation, and black indicating no change in the expression. **D,** Gene expression dynamics inspector (GEDI) 11-by-10 clustering analysis for the 3,258 genes that were differentially expressed in at least one comparison. Genes with similar expression values were grouped within the same tile. Expression values are color-coded, with red tiles indicating upregulation, blue tiles indicating downregulation, and yellow tiles indicating no change in the expression.

points (1,482, 1,662, and 1,816 for the SN, VIGS Prot, and SHR comparisons, respectively), than at the early time points (33, 772, and 1,371, respectively). In general, approximately equal numbers of genes were either induced or repressed at the different time points in all the comparisons. Relatively few statistically significant genes were identified for SN at 7 dpi, most probably due to subtle differences in gene expression in this comparison at early times of infection. Thus, for the SN comparison, we focused on the list of genes altered at 11 dpi.

Venn analysis of selected genes showed that treatments caused both common and specific changes in host gene expression (Fig. 2A and B). There was substantial overlap in the genes altered in each comparison and, in most cases (98%), the observed expression changes were in the same direction. In all, 60.2% (893/1,482) and 69.2% (1,026/1,482) of statistically significant genes identified from the SN comparison also were altered in the SHR comparison at the early (24 hts) and late (72 hts) time points, respectively. In contrast, expression of a relatively smaller number of genes was shared between SN and VIGS Prot at the early (4 dai, 37%) and late (8 dai, 50.9%) time points. A similar trend in overlapping regions was observed when comparing the total number of differentially regulated genes between the three comparisons across time (data not shown).

Hierarchical clustering (HCL) was used to group the entire data sets from the five comparisons by the similarity of their overall gene expression profiles (Fig. 2C). The expression profiles corresponding to samples with PCD triggered by proteasome silencing at 4 and 8 dai clustered together, apart from samples representing PCD induced by compatible and incompatible viral infections. Remarkably, samples from SHR 24 hts and SN 11 dpi were grouped together, indicating a closer relationship in the changes of relative transcript abundance between these responses compared with those altered by SHR at 72 hts.

The similarity between responses observed at the late stages of a compatible interaction leading to SN and those that occur at early stages of an incompatible interaction was further depicted using a self-organizing map (SOM) clustering algorithm (gene expression dynamics inspector [GEDI]) (Eichler et al. 2003). GEDI uses SOM to express complex data sets as mosaic images that are characteristic for each sample. Each mosaic tile represents a group of genes that are expressed at similar levels across different experimental conditions which, in turn, are similar in expression to the surrounding mosaic tiles. This creates an image of the transcriptome that allows its analysis as an entity by simple visualization. Because the assignment of genes to the tiles is universal for the entire set of expression profiles, GEDI maps can be directly compared with each other. Therefore, the expression profile of differentially expressed genes in all five microarray comparisons were visualized as GEDI maps, each consisting of an 11-by-10 mosaic (Fig. 2D). Consistent with HCL data, visual inspection of the GEDI maps readily confirmed that SN displays significant feature similarities, although with differences, to SHR 24 hts, based on the fine structure of the patterns of deregulated genes. The visual patterns of the GEDI maps of these samples remained similar when the analysis was performed with a wide range of SOM parameters (data not shown).

Functional analysis of differentially expressed genes.

We applied a Java-based platform, the Cytoscape plug-in ClueGO (Bindea et al. 2009), to determine which Gene Ontology (GO) terms within biological process categories were statistically overrepresented (hypergeometric test, $P < 0.005$) in each set of differentially expressed genes that were up- or downregulated by the different experimental comparisons. Overall,

overrepresentation analysis on the set of genes altered by SHR 24 hts, SHR 72 hts, SN 11 dpi, VIGS Prot 4 dai, and VIGS Prot 8 dai identified 68, 64, 56, 42, and 58 functional categories, respectively (Supplementary Table S2). Interestingly, of the 56 GO categories overrepresented in SN, 82 and 77% were also identified in SHR at 24 and 72 hts, respectively (Supplementary Fig. S1). In contrast, a smaller number of GO categories were shared between SN and VIGS Prot at 4 and 8 dai (46 and 55%, respectively), indicating a biological significance for the clustering analysis described above. Most of the similarity in biological processes overrepresented in SN and SHR comparisons came from repressed GO categories. No GO category was overrepresented in the data set from SN at 7 dpi. Analysis with another algorithm, BiNGO (Maere et al. 2005), gave overlapping results to the ones obtained by ClueGO as to which biological processes and pathways are affected in the three different experimental comparisons (data not shown).

ClueGO integrates GO terms that have similar associated genes using kappa statistics and creates functionally organized networks of GO terms. The networks of GO terms that were enriched in the different experimental comparisons illustrated the complexity of the transcriptional response, with a large number of pathways and processes being affected in all three PCD responses (Figs. 3 and 4). Even within the selected pathways and processes that will be presented below, it is out of the scope of this article's main text to present and discuss all aspects.

Analysis of downregulated genes.

Overrepresentation analysis revealed a set of functionally grouped networks of enriched GO categories that were commonly repressed by all three comparisons. These included photosynthesis-related processes, cell wall remodeling, glucan metabolism, and gibberellic acid signaling.

Photosynthesis and, to a lesser extent, other related biochemical processes, i.e., chlorophyll biosynthesis, photosynthetic electron transport chain, glycine decarboxylation (photorespiration), thiamine biosynthesis (involved in chlorophyll biosynthesis as a cofactor in isopentenyl diphosphate biosynthetic process), and ferredoxin metabolism—were revealed by ClueGO as the most prominent GO networks being affected in several of our data sets (Fig. 3). The overrepresentation of the networks of

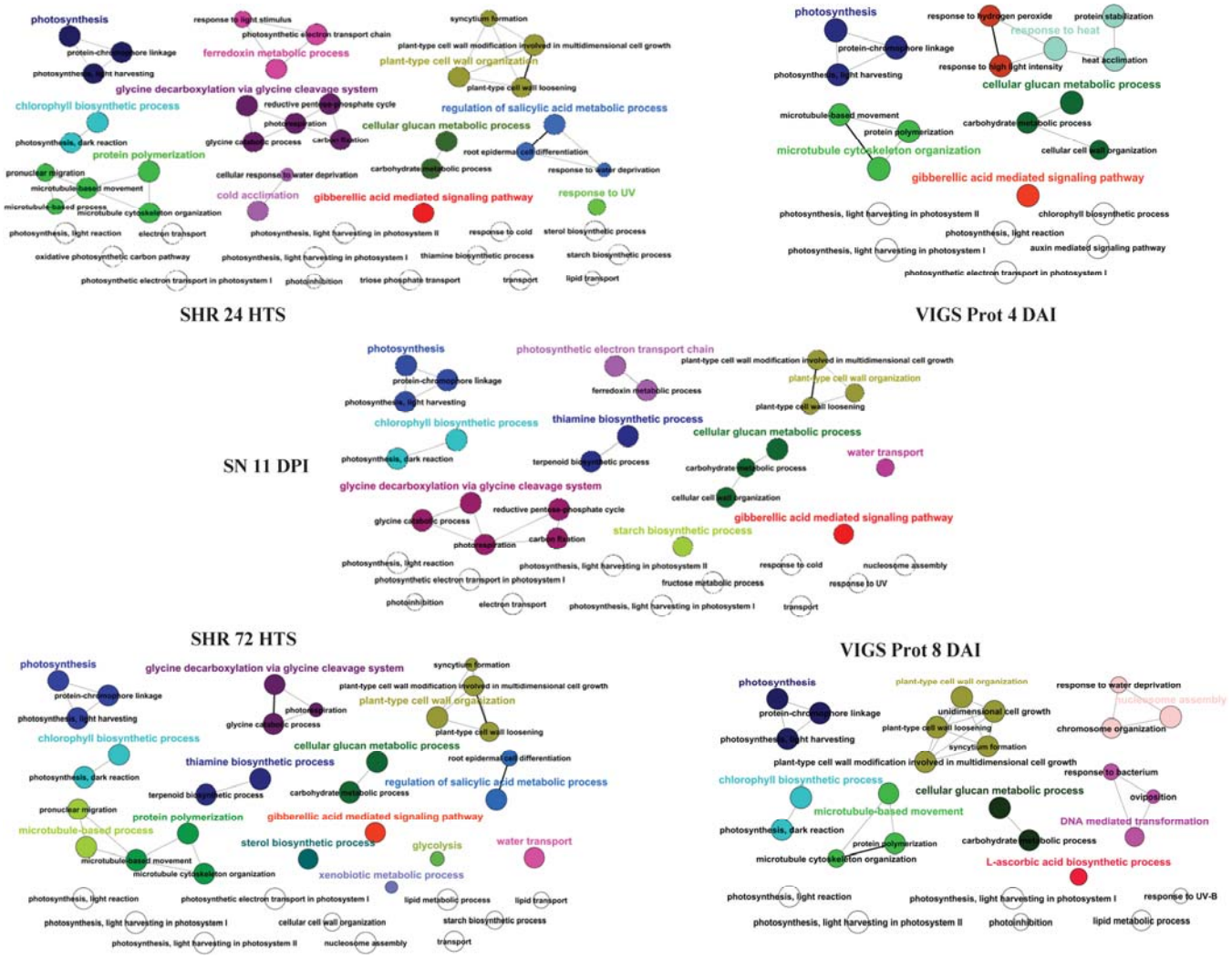

Fig. 3. Network representations of enriched Gene Ontology (GO) categories among genes induced in systemic necrosis (SN), systemic hypersensitive response (SHR), and virus-induced gene silencing of proteasome (VIGS Prot) comparisons at early (24 h after temperature shift [HTS] and 4 days after infiltration [DAI], respectively) and late (11 days postinoculation [(DPI], 72 HTS, and 8 DAI, respectively) stages of infection. Representations generated by ClueGO of functionally grouped networks of biological process GO categories identified as enriched among the induced data sets derived from the different experimental comparisons. GO terms are represented as nodes based on their kappa score level (≥0.3). Biological processes are color-coded as indicated on the figure. The label of the most significant term is used as leading group term. Multicolored networks contain GO terms shared by more than one functional group. The node size represents the term enrichment significance. The not-grouped terms are shown in white.

GO terms related to photosynthesis in data sets from both SN and SHR was wider and of greater significance than in those from VIGS Prot, indicating a deeper impact of PCD induced by compatible and incompatible viral infections on chloroplastic metabolism (group *P* value). Furthermore, the significance of the GO network photosynthesis (Fig. 3, dark-blue network), the most abundant category of repressed genes, was greater in SN (group *P* value, 3.8E-101) and SHR at 24 hts (6.3E-100) than in SHR at 72 hts (2.0E-72). The same trend was observed for the GO network glycine decarboxylation, the other network related to chloroplast metabolism commonly repressed in SN and SHR data sets (Fig. 3, purple network).

Because overrepresentation analysis does not take into account amplitudes of transcriptional changes, HCL on all 118 genes within the GO network photosynthesis that were differentially expressed in at least one comparison was used to cluster genes and treatments based on gene expression profiles, to further study the behavior of these genes. Overall, the repression of photosynthesis-related genes was stronger in plants infected by either the compatible or incompatible virus than by depletion of proteasome function (Supplementary Fig. S2; Supplementary Table S3). In addition, the profiles of SN and SHR at 24 hts were clustered together and separately from that of SHR at 72 hts. Thus, the repression of photosynthesis-related genes in a compatible interaction that leads to SN is more similar to that found in an incompatible interaction at the early than at the late stages of infection.

Another significantly overrepresented subset for which transcript abundance decreased in response to all three comparisons was that of genes postulated to play a role in the loosening and rearrangement of the cell wall (Cosgrove 2005). These genes were grouped into three networks of enriched GO categories (i.e., plant-type cell wall organization, cellular glucan metabolic process, and gibberellic acid mediated signaling pathway) (Fig. 3, gray, dark-green, and red networks, respectively), and included cell-wall-modification enzymes (endoglucanases, polygalacturonases, and xyloglucan endotransglycosylases) as well as other genes related to cell wall dynamics (expansins and extensions). There was no clear bias in the significance of these GO networks toward any of the different comparisons.

In addition to the commonly repressed genes, ClueGO identified a group of GO categories that were overrepresented exclu-

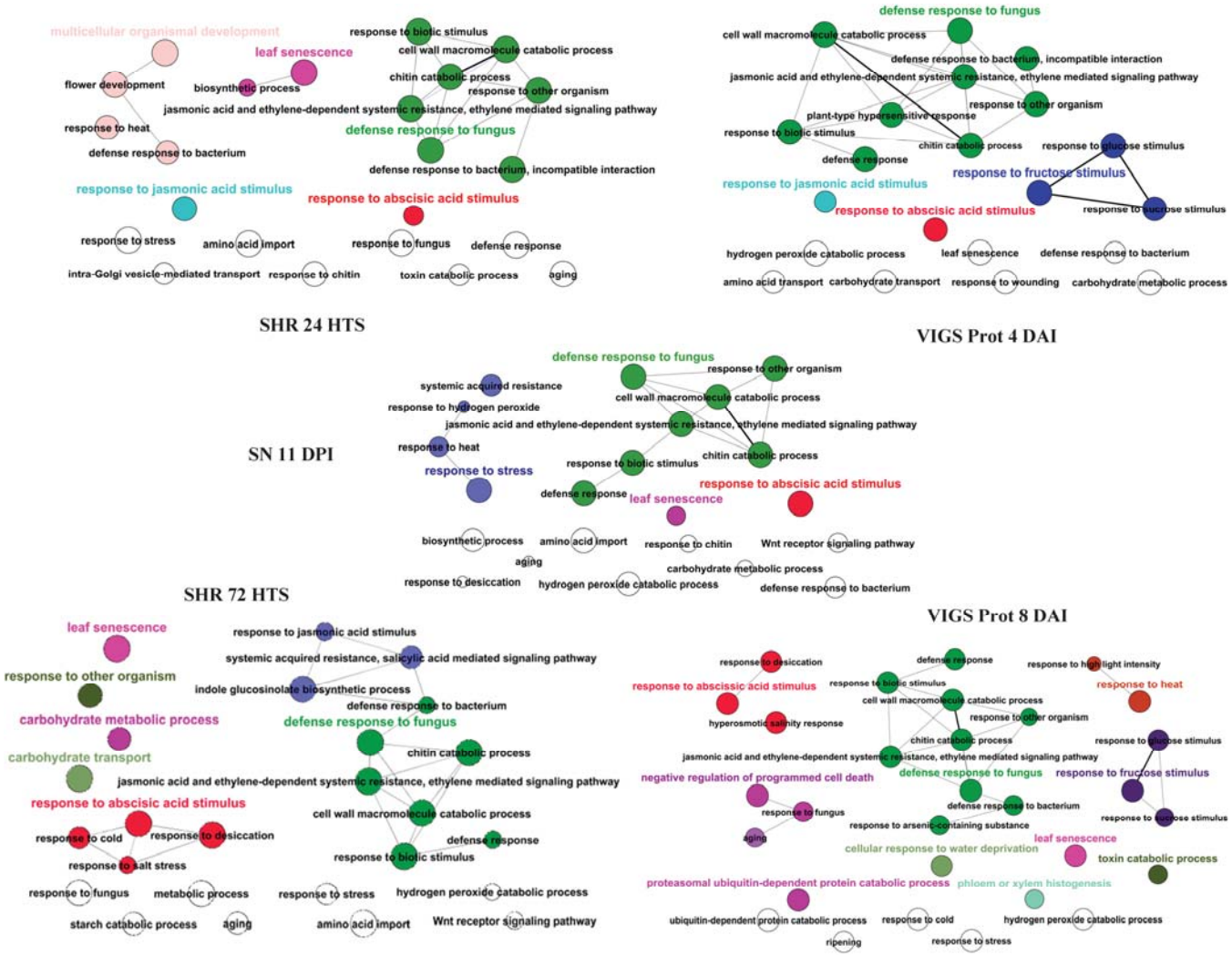

Fig. 4. Network representations of enriched Gene Ontology (GO) categories among genes repressed in systemic necrosis (SN), systemic hypersensitive response (SHR), and virus-induced gene silencing of proteasome (VIGS Prot) comparisons at early (24 h after temperature shift [HTS] and 4 days after infiltration [DAI], respectively) and late (11 days postinoculation [DPI], 72 HTS, and 8 DAI, respectively) stages of infection. Representations generated by ClueGO of functionally grouped networks of biological process GO categories identified as enriched among the repressed data sets derived from the different experimental comparisons. GO terms are represented as nodes based on their kappa score level (≥0.3). Biological processes are color-coded as indicated on the figure. The label of the most significant term is used as leading group term. Multicolored networks contain GO terms shared by more than one functional group. The node size represents the term enrichment significance. The not-grouped terms are shown in white.

sively in any of the different comparisons. Microtubule-related processes (light green network) were downregulated by PCD induced by VIGS Prot and SHR at both time points but not by SN. Genes in these GO categories include FtsZ-like proteins and several subunits of α- and β-tubulins.

A group of genes exclusively overrepresented in the SHR comparison were enclosed in the GO term regulation of SA metabolic process. They encode enzymes with endochitinase activities which have been involved in cell wall expansion and responses to abiotic stresses.

The GO networks' response to heat- and DNA-mediated transformation were overrepresented exclusively in data sets from VIGS Prot at 4 and 8 dai, respectively. Although nucleosome assembly was repressed in all three comparisons, the significance of this GO term was greater in VIGS Prot 8 dai than in SHR 72 hts and SN. These three GO terms included 11 heat shock proteins, DNA-binding proteins, and different types of histones, respectively. Other repressed GO terms with few associated genes were those related to different types of abiotic stresses (cold, drought, and UV light) and several types of biosynthetic processes.

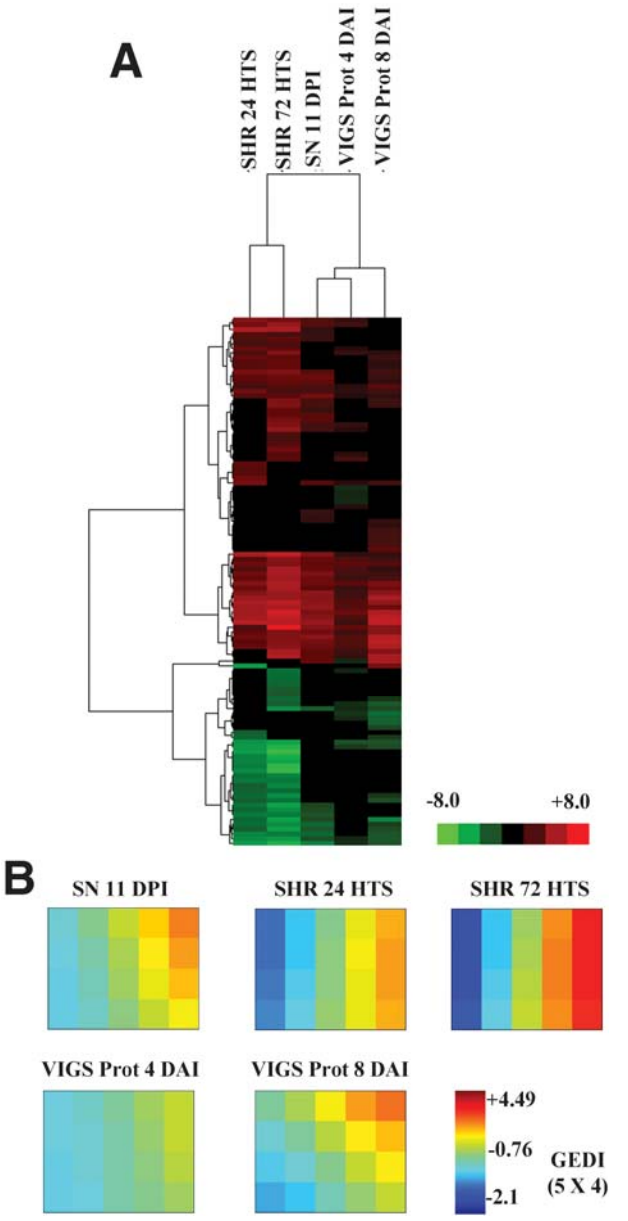

Fig. 5. Transcriptional regulation of the 110 genes within the Gene Ontology network defense response to fungus that were identified in overrepresentation analyses in systemic necrosis (SN), systemic hypersensitive response (SHR), and virus-induced gene silencing of proteasome (VIGS Prot) comparisons at early (24 h after temperature shift [HTS] and 4 days after infiltration [DAI], respectively) and late (11 days postinoculation [DPI], 72 HTS, and 8 DAI, respectively) stages of infection. **A,** Hierarchical cluster analysis of the expression profiles for the 110 genes that were differentially expressed in at least one comparison was performed by the Cluster 3.0 program. Expression values are color-coded, with red indicating upregulation, green indicating downregulation, and black indicating no change in the expression. **B,** Gene expression dynamics inspector (GEDI) 5-by-4 clustering analysis for the 110 genes that were differentially expressed in at least one comparison. Genes with similar expression values were grouped within the same tile. Expression values are color-coded, with red tiles indicating upregulation, blue tiles indicating downregulation, and yellow tiles indicating no change in the expression.

Analysis of upregulated genes.

In data sets from all three comparisons, induced genes predicted to encode proteins that are related to defense responses were in the most highly overrepresented GO categories (green network) (Fig. 4). Analysis of the affected GO terms indicates that the different types of PCD lead to transcriptional changes that consist of the activation of multiple responses to biotic stimuli or the activation of mechanisms that are common to several biotic stresses. The significance of overrepresentation of this network of enriched GO categories varied across time, with lower *P* values found at the early time points in both SHR (1.3E-13) and VIGS Prot (1.1E-14) comparisons compared with the late time points (1.9E-11 and 2.9E-8, respectively). The significance of the defense-related GO network in the SN data set (6.2E-14) was more similar to the early time points from the other comparisons. Interestingly, HCL of all 110 genes within the GO network defense response to fungus that were differentially expressed (up or down) in at least one comparison showed that the profile of SN was more similar to the profiles of VIGS Prot at both time points than to those of SHR (Fig. 5). Genes in these GO categories comprise pathogenesis-related (PR) proteins, basic chitinases, mitogen-activated protein kinase, WRKY transcription factors, and enzymes implicated in the biosynthesis of plant oxylipins, among others. It should be stressed that many of the differences between SN and SHR came from the 26 and 33 genes which were not differentially expressed in SN but were up- or downregulated in SHR at 24 and 72 hts, respectively (40% of all the deregulated, defense-related genes in SHR at both time points).

A variety of plant hormones has been implicated in the regulation of cell death because the hormones modulate plant responses to a wide array of stress conditions (Hoeberichts and Woltering 2003). In this study, three different hormone signaling pathways—that is, response to ABA (Fig. 4, red) response to JA (light-blue network), and systemic acquired resistance (SAR) (middle blue)—were found to be overrepresented in induced data sets at any time point. In addition, the GO term JA and ethylene-dependent systemic resistance were present in all three comparisons in the GO network defense response to fungus (green). Again, HCL of all 81 genes (75% of which did not overlap with defense response genes) within the GO terms related to hormone signaling showed that the expression profile of SN clustered with those of VIGS Prot at both time points rather than with those of SHR (Supplementary Fig. S3). Together, these results suggest that defense- or hormone-related responses to a compatible virus infection that leads to SN bear a much closer resemblance to PCD induced by depletion of proteasome function than to PCD induced by an incompatible virus.

Other GO terms commonly induced by all three comparisons were leaf senescence and response to stress or heat. Many of the genes included in the GO network multicellular organismal

development (SHR 24 hts) correspond to genes involved in stress or heat responses. The GO category carbohydrate metabolism was commonly overrepresented in SN and SHR data sets. On the other hand, two GO networks exclusively overrepresented in VIGS Prot were related to response to sugars (dark blue) and proteasomal proteins (pink), the last one likely being a plant response to cope with the shutdown in proteasome function (Lundgren et al. 2003).

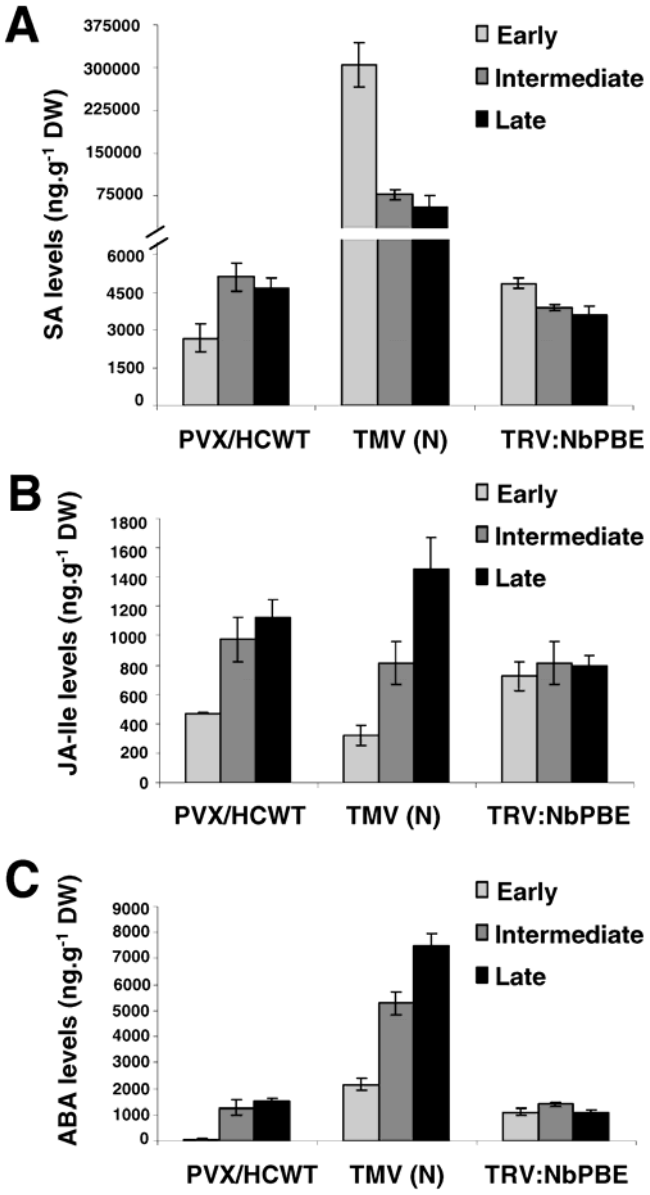

Fig. 6. Hormone levels in *Nicotiana benthamiana* plants after infection by necrosis-inducing pathogens. Leaves were collected from plants at different time points after inoculation with *Potato virus X* (PVX)/HCWT, *Tobacco mosaic virus*-based vector expressing free green fluorescent protein (TMV-GFP), or TRV:*NbPBE* and **A,** free salicylic acid (SA); **B,** jasmonic acid-Ile (JA-Ile); and **C,** abscisic acid (ABA) levels were determined in freeze-dried material by high-performance liquid chromatography mass spectrometry. Based on the progress of the necrotic symptoms induced by the respective pathogens, harvesting of leaf tissue for hormone determinations were done at 4, 6, and 8 days after TRV:*NbPBE* infiltration; 7, 9 and 11 days after PVX/HCWT inoculation; and 24, 48, and 72 h after temperature shift in TMV-GFP-infected plants. These sampling time points correspond to early, intermediate, and late stages of infection, respectively. Amounts of hormones in leaves of mock-inoculated plants were negligible compared with plants infected with necrosis-inducing viruses. Data represent the means ± standard errors of three replicates, each consisting of three to seven plants that received the same treatment. DW = dry weight.

Accumulation profiles of SA, JA-Ile, and ABA and hormone-responsive genes.

To investigate the dynamics of SA, JA-Ile conjugate, and ABA during the different types of PCD analyzed in this study, we monitored the accumulation of these hormones after infection by either necrosis- or non–necrosis inducing pathogens across time. Overall, the magnitude of hormone accumulation was higher in plants infected with PVX/HCWT, TRV:*NbPBE*, or TMV-GFP (*N* plants) than during infections with PVX/HCLH, TRV:00, or TMV-GFP (wild-type plants), respectively (Supplementary Fig. S4). When comparing hormone accumulation between necrosis-inducing viruses, SA, JA-Ile, and ABA tend to accumulate to similar levels, although with different kinetics, in both PVX/HCWT- and TRV:*NbPBE*-infected plants (Fig. 6). Infection by TMV-GFP, however, induced a much higher increase in the production of SA compared with infections by PVX/HCWT and TRV:*NbPBE*, which ranged from 113- and 62-fold increase at early time points to 12- and 15-fold at late time points, respectively. A moderate raise in ABA levels was also detected in TMV-GFP-infected plants compared with PVX/HCWT (fivefold, late time point) and TRV:*NbPBE* (sevenfold) infections. Quantification of SA, JA-Ile, and ABA revealed negligible amounts of hormones in leaves of mock-inoculated plants compared with plants infected with necrosis-inducing viruses (data not shown). These results further confirm microarray data regarding similarities in expression patterns of defense- or hormone-related genes between SN and VIGS Prot, and suggest that SA signaling is a major contributor to the differential regulation of defense response in SHR.

To examine how much the patterns of hormone production during each comparison correlate with a coordinate activation of SA-, JA-, or ABA-responsive genes, we analyzed the expression of well-characterized marker genes by qRT-PCR at early stages of infection. These genes included *PR-1* (SA responsive) and *ABA2* (ABA responsive), among others. Previous analysis had shown significant increases in the expression of genes associated with oxylipin production in plants doubly infected with PVX and PVY (García-Marcos et al. 2009). To test the possibility that increased JA-Ile in PVX/HCWT-infected plants contributed to the enhanced accumulation of oxylipin biosynthesis genes, we treated healthy *N. benthamiana* plants with exogenous JA. RT-PCR analysis showed that *9-LOX, 13-LOX*, α-*dioxygenase 1* (α-*DOX1),* and *AOS* gene expression were, indeed, induced in JA-treated plants (Supplementary Fig. S5). Thus, all these JA-responsive genes as well as an ethylene-responsive gene, *ACO2*, were included in the analysis. As an independent validation of hormone measurements, we used the same RNA preparations analyzed in microarray experiments.

The results indicated that, in general, the expression patterns of the marker genes correlated well with the accumulation patterns of the hormonal signals in each comparison, with a significant increase in plants infected with necrosis-inducing pathogens compared with plants infected with non–necrosis inducing pathogens. The exception was *ABA2*, which was only significantly upregulated in PVX/HCWT-infected plants compared with PVX/HCLH infection. The differential accumulation of SA in SHR was reflected by the disproportional accumulation of *PR-1* in necrosis- versus non–necrosis inducing conditions (32-fold increase), as compared with SN (2.5-fold increase) and VIGS Prot (sevenfold increase) comparisons.

Silencing of *NbCOI1* accelerates cell death induced by PVX/HCWT.

Research on host signaling upon pathogen attack has established the primacy of two pathways in plants, one involving SA and the other involving JA (Whitham et al. 2006). It is gen-

erally believed that most plant responses to viruses are mediated by SA signaling. However, not much information about the role of jasmonates on viral infection is available. To assess a functional role of JA signaling in the SN induced by PVX/HCWT, we silenced *COI1* in *N. benthamiana* by VIGS. COI1 participates in JA perception and regulates gene expression through its interaction with transcriptional repressors (Chini et al. 2009). *N. benthamiana* plants were infiltrated with a recombinant vector carrying a fragment of *NbCOI1* (TRV:*NbCOI1*) or TRV:00 as a control. At 10 dai, plants were either mock inoculated or challenge inoculated with PVX/HCWT in upper, noninfiltrated leaves. *NbCOI1* silencing efficiency was examined by qRT-PCR at 10 dai in mock-inoculated plants (Fig. 7A) and at 9 dpi with PVX/HCWT (19 dai) (Fig. 7G, left

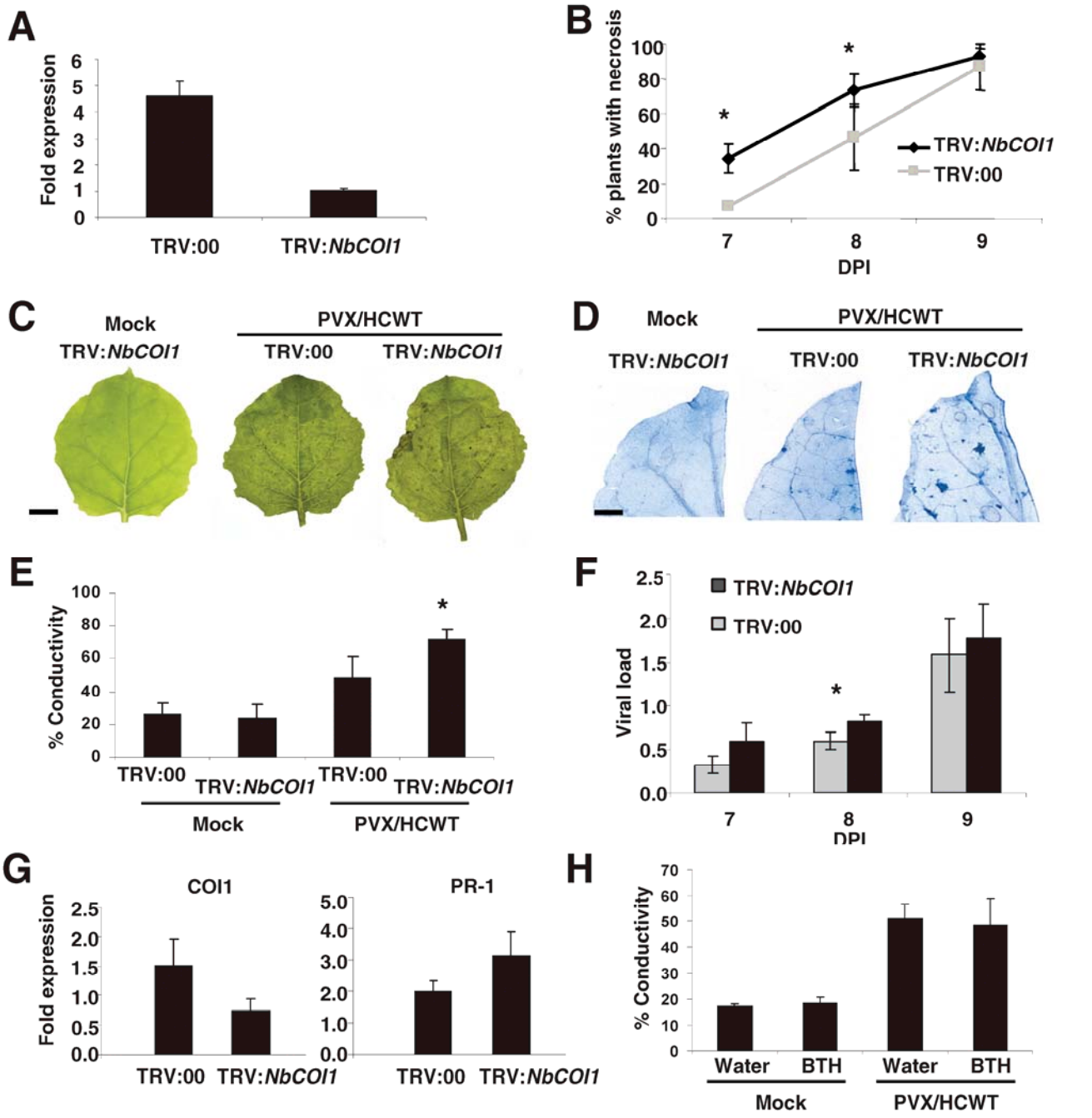

Fig. 7. Silencing of *Nicotiana benthamiana coronatine insensitive1* (*NbCOI1*) results in accelerated cell death induced by *Potato virus X* (PVX)/HCWT infection. Three-week-old *Nicotiana benthamiana* plants were infiltrated with *Agrobacterium* spp. containing TRV:*NbCOI1* or TRV:00 (vector control). **A,** Relative expression of *NbCOI1* estimated by quantitative reverse-transcriptase polymerase chain reaction (qRT-PCR) in *N. benthamiana* plants 10 days after infiltration (dai). **B,** Agroinfiltrated plants were mock inoculated or inoculated with PVX/HCWT at 10 dai and scored for the appearance of necrosis. The experiment was repeated twice, independently, with 45 to 60 plants of each treatment. **C,** Representative necrotic symptoms displayed in *NbCOI1*-silenced and control plants at 9 days postinoculation (dpi). Scale bars = 1 cm. **D,** Uppermost leaves of control and *NbCOI1*-silenced plants were stained with trypan blue to detect cell death at 9 dpi. Scale bars = 0.5 cm. **E,** Leaf discs were excised and assayed for electrolyte leakage at 11 dpi. **F,** qRT-PCR was used to analyze PVX/HCWT accumulation in control and *NbCOI1*-silenced plants at 7, 8, and 9 dpi. **G,** Relative expression of *COI1* (left panel) and *PR-1* (right panel) estimated by qRT-PCR in control and *NbCOI1*-silenced plants at 9 dpi (19 dai). **H,** Benzo (1,2,3) thiadiazole-7-carbothioic acid *S*-methyl ester (BTH), or water solution as a control, was applied to leaves that were mock inoculated or inoculated with PVX/HCWT. Leaf discs were excised and assayed for electrolyte leakage at 11 dpi. Data represent the means ± standard errors of at least three replicates. Differences from control values were significant at $P < 0.05$ (*), according to Duncan's multiple range test.

panel). The results showed significant knockdown of *NbCOI1* transcripts in both mock- and PVX/HCWT-inoculated, TRV:*NbCOI1*-infiltrated plants compared with the controls (TRV:00). Partial suppression of *NbCOI1* expression in mock-inoculated, *NbCOI1*-silenced plants caused slightly retarded plant growth.

Typical chlorotic mosaic symptoms were observed simultaneously in both *NbCOI1*-silenced and control plants at 7 dpi with PVX/HCWT. Symptom severity was evaluated by recording the development of necrotic patches on leaves from 7 to 9 dpi (Fig. 7B). At 7 dpi, less than 10% of TRV:00-infiltrated plants displayed necrotic patches in leaves, whereas 35% of *NbCOI1*-silenced plants showed necrosis (significant difference, $P < 0.05$). By 9 dpi, the number of plants affected by necrosis reached 90% in both control and *NbCOI1*-silenced plants, although the development of cell death in *NbCOI1*-silenced leaves was significantly faster than that in nonsilenced control leaves (Fig. 7C). These results were obtained in three biological replicates with 30 to 40 plants in each treatment. Mock-inoculated, *NbCOI1*-silenced plants remained free of necrotic symptoms throughout the trial period. Consistent with these observations, trypan blue staining and electrolyte leakage measurement, as a quantitative assessment of the extent of cell damage, revealed extensively enhanced cell death in *NbCOI1*-silenced leaves compared with nonsilenced control leaves (Fig. 7D and E). To examine whether the enhanced cell death phenotype was associated with changes in accumulation of PVX/HCWT, we measured the amount of virus in systemically infected leaves from *NbCOI1*-silenced and control plants (Fig. 7F). qRT-PCR analysis showed that PVX/HCWT trends to accumulate to higher levels in *NbCOI1*-silenced plants at early times of infection, with significant differences observed at 8 dpi ($P < 0.05$).

Previous studies had provided evidence that high activation of the SA signaling pathway is required for the SN response induced by several compatible virus infections (Atsumi et al. 2009; Kim et al. 2008). Our qRT-PCR analysis shows that *PR-1* gene expression was, indeed, differentially induced in PVX/HCWT-infected, *NbCOI1*-silenced plants when compared with infected nonsilenced controls, suggesting that JA and SA signaling act in an antagonistic manner in *NbCOI1*-silenced plants (Fig. 7G, right panel). To test whether an activated SA-signaling pathway affected the pathogenicity of PVX/HCWT, we treated wild-type *N. benthamiana* plants with water or the SA analog benzo (1,2,3) thiadiazole-7-carbothioic acid *S*-methyl ester (BTH) (Fiedrich et al. 1996). As expected, BTH treatment induced *PR-1* expression in both local and upper leaves (data not shown). BTH- and water-treated plants were then inoculated with PVX/HCWT and induction of cell death was monitored in systemic leaves of these plants. We found that there was no significant effect on the development of necrotic patches that could be attributed to treatment with BTH. Furthermore, electrolyte leakage measurement did not detect significant differences in the extent of cell damage between the water- and the BTH-treated plants (Fig. 7H). PVX/HCWT accumulation was not affected by BTH treatment (data not shown). These results showed that the enhanced necrosis in *NbCOI1*-silenced plants infected with PVX/HCWT was likely not due to activation of SA-dependent responses.

DISCUSSION

PCD is involved in PVX-*Potyvirus* synergism.

Previous studies have shown that several hallmarks of HR, such as nuclear DNA degradation, ROS production, and expression of defense-related genes, were associated with the induction of SN in several compatible plant–virus interactions (Komatsu et al. 2010; Xu and Roossinck 2000). We previously demonstrated that synergistic infection by PVX and PVY induced a more severe oxidative stress in *N. benthamiana* leaves compared with single infections, which correlated with the misregulation of defense-related genes (García-Marcos et al. 2009). The present study also showed that DNA degradation in *N. benthamiana* plants after infection with PVX/HCWT led to SN. Thus, PCD is thought to be involved not only in HR-associated resistance reaction to incompatible virus but also in necrosis disease induced by PVX–*Potyvirus*-associated synergisms.

One interesting aspect revealed in our study is that virus accumulation was greater in leaf tissues undergoing necrosis than in non–necrosis inducing conditions in all three cases of PCD. Although these variations in viral loads may contribute to the differential gene expression observed within each comparison, it highlights an attribute common to the experimental systems (i.e., PCD was correlated with increased virus accumulation). González-Jara and associates (2005) demonstrated that wild-type PPV HC-Pro could suppress RNA silencing in an *A. tumefaciens*–mediated transient assay in *N. benthamiana*, whereas the PPV $HCL_{134}H$ mutant showed no such activity. Thus, it is likely that RNA silencing suppression activity can explain, at least in part, the enhanced virus accumulation associated with the late stages of PVX/HCWT infection. Similarly, Atsumi and associates (2009) reported that a reduced ability to induce SN in plants infected by HC-Pro mutants of *Clover yellow vein virus* was accompanied by decreased virus accumulation, which correlated with a reduced suppressor activity of the mutated proteins. However, SN was not associated with enhanced levels of virus titers in *N. clevelandii* infected with *Cauliflower mosaic virus* (Király et al. 1999). In plants, the proteasome harbors a ribonuclease activity which has been shown to specifically target viral RNAs (Ballut et al. 2005; Dielen et al. 2011). Thus, it is tempting to speculate that, in *NbPBE*-silenced plants, the inhibition of proteasome function would allow TRV:*NbPBE* to accumulate beyond the normal host-imposed limits. The molecular mechanism associated with the greater accumulation of TMV-GFP in *N*-transgenic plants compared with the wild-type genotype is unknown.

Changes in gene expression during SN are delayed when compared with those during SHR.

We found few (33) differentially expressed genes in SN at early stages of infection but over 1,400 at later stages, when necrosis appeared in systemically infected leaves. This dynamics is completely different from the dynamics observed in SHR or VIGS Prot, where a very fast and extensive transcriptome change occurred at early stages of infection (1,371 and 772 differentially regulated genes, respectively). Because rather similar differences in viral titers (two- to threefold) were detected in each comparison after infection by either necrosis- or non–necrosis inducing pathogens at early time points, it is unlikely that such large variation in the number of differentially expressed genes between the compatible and the incompatible interaction was attributable only to differences in viral loads within each comparison. Instead, this observation suggests that host responses during an incompatible virus interaction are more robust than those in a compatible virus interaction that leads to SN at early stages of infection. This is likely so because plant cells do not recognize the pathogen until the disease has progressed considerably, or due to temporal suppression of plant defense mechanisms. A similar response was reported in *Arabidopsis thaliana* during compatible and incompatible interactions with the bacterial pathogen *Pseudomonas syringae* (Tao et al. 2003). Nevertheless, differential expression of a set of hormone-responsive genes was detected in SN at early stages of infection by qRT-PCR, as expected by the

increased levels of SA, JA, and ABA measured at this time point.

Our results are in general agreement with other studies showing that responses to compatible pathogens lag behind those seen in incompatible interactions (Jones and Dangl 2006; Tao et al. 2003). The overall expression profile in response to SN at late stages of infection was closer to that of SHR at the early time point than at the late time point, and clearly differed from those of VIGS Prot at both time points. GO enrichment analysis and further examination of sets of misregulated genes by clustering analysis revealed that similarities between SN and SHR at 24 hts came from repressed genes, being particularly evident in the case of photosynthesis-related genes. Repression of photosynthesis and chloroplast metabolism in general is a common host response to compatible and incompatible pathogens (Bolton 2009). Previously, it was reported that PVX–PVY infection promoted the peroxidation of lipids, in parallel with an increased generation of O_2^- in chloroplasts (García-Marcos et al. 2009). The generation of ROS in chloroplasts has been described to play an important role in the signaling for or execution of HR cell death in plants (Liu et al. 2007). Thus, ROS signaling could be considered an important part of cell death processes, resulting in the rapid cell-death phenotype in HR during the incompatible interaction or the delayed disease-related cell death during the compatible interaction. A decrease in the photosynthetic rate by transcriptional repression in both compatible and incompatible interactions may attempt to protect the photosynthetic apparatus against oxidative damage or, alternatively, be a consequence of stress responses caused by virus infections (Bolton 2009).

Other interesting changes observed in this study were the significant repression of cell-wall-related genes in all three cases of PCD. This gene group is known to be a major determinant of cell morphogenesis and growth in plants (Cosgrove 2005). Thus, decreased expression of cell-wall-modification enzymes is consistent with disease symptoms, such as the stunted growth observed in plants infected with PVX/HCWT, TRV:*NbPBE*, or TMV-GFP. This is in general concurrence with previous findings that cell-wall-related transcripts were downregulated in plants infected with diverse RNA viruses (Shimizu et al. 2007; Yang et al. 2007).

SN-induced defense and hormonal responses share similarities to those induced by depletion of proteasome.

All three *N. benthamiana*–virus interactions that led to PCD caused a considerable increase in SA, JA, and ABA production, and were associated with the subsequent activation of defense-related and hormone-responsive genes. It is noteworthy, however, that expression profiles of defense- or hormone-related genes in response to SN were more closely related to profiles in response to depletion of proteasome function than to those elicited by SHR. Biochemical measurement of phytohormone levels and expression analysis of marker genes supported these findings, suggesting that SA regulates the differential response in SHR compared with SN. A marked increase of SA is required for the induction of SAR that occurs during resistance response to incompatible viruses (Lewsey et al. 2009). Thus, even though production of SA and expression of PR-1 was increased at early stages of PVX/HCWT infection, this was not effective in restraining virus multiplication and spread to upper parts of the plant. Furthermore, the activation of SA signaling by application of BTH on wild-type plants did not affect the pathogenicity of PVX/HCWT, indicating that the SA-mediated, defense-like response that is induced during compatible infections has very little effect, if any, on pathogenicity (Huang et al. 2005).

The altered expression of defense- or hormone-responsive genes observed in PVX/HCWT-infected plants may be linked to the interference of HC-Pro with multiple RNA silencing pathways (Soitamo et al. 2011). However, the expression of the *HC-Pro* gene alone does not account for the ample transcriptome changes observed in PVX/HCWT infection. Soitamo and associates (2011) analyzed the transcriptional response of *N. tabacum* leaves which constitutively express the HC-Pro derived from PVY in the Agilent microarray used in this study. Comparison with our data showed that only a small pool of genes (48 of 748) was commonly misregulated in both transcriptomes. Thus, additional layers of altered regulatory circuits may exist in virus-infected plants that modulate the extensive transcriptome reprogramming observed in PVX/HCWT infection. Interestingly, it was reported that HC-Pro from *Lettuce mosaic virus* (LMV) could bind the proteasome and inhibit its 20S endonuclease activity, while its proteolytic activity was slightly stimulated (Ballut et al. 2005). The 20S proteasome is involved in antiviral responses in animals and plants (Dielen et al. 2010). Indeed, a knockout mutant of *Arabidopsis* PAE proteasome subunit exhibited increased susceptibility to LMV (Dielen et al. 2011). Thus, *Potyvirus* spp. could target host defense mechanisms through interference with the proteasome mediated by HC-Pro. These alterations on proteasome activities would not necessarily provide an advantage to the virus but may have adverse effects on cellular homeostasis that contribute to disease-symptom development. In our study, *NbPBE* silencing and subsequent disruption of proteasome function could partially mimic HC-Pro action on proteasome activities, allowing virus to accumulate beyond the normal host-imposed limits and induce a somehow similar defense or hormone response in both TRV:*NbPBE*- and PVX/HCWT-infected plants.

***COI1* negatively regulates cell death induced by PVX/HCWT.**

We have shown that silencing of *COI1* accelerated cell death induced by PVX/HCWT in the susceptible host *N. benthamiana*. Accelerated necrosis may be interpreted as a consequence of the slightly increased accumulation of virus observed in *NbCOI1*-silenced plants. Thus, COI1 interferes somehow with infection by PVX/HCWT, indicating that viral multiplication is partly restrained even in SN induced by a compatible virus infection. Liu and associates (2004) reported that VIGS of *COI1* led to loss of HR resistance to TMV in *N*-transgenic *N. benthamiana* plants. This suggests that plant responses to compatible and incompatible interactions share a common step mediated by COI1. COI1 is part of the Skp1-Cullin-F-box (SCF) E3 ubiquitin ligase complex SCF^{coi1} that participates in JA perception (Chini et al. 2009). Interestingly, SGT1, an interactor of SCF complexes, is required for the restraint of viral accumulation in the SN caused by *Plantago asiatica mosaic virus* in *N. benthamiana* (Komatsu et al. 2010). Thus, convergent routes associated with the ubiquitin-proteasome-dependent pathway may be operating in mediating partial inhibition of virus multiplication during compatible plant–virus interactions.

We previously demonstrated that downregulation of α-*DOX1* by VIGS led to an attenuated cell death response at early stages of PVX–PVY infection (García-Marcos et al. 2009). α-*DOX1* is involved in the oxygenation of fatty acids into reactive 2-hydroperoxides and represents an oxylipin biosynthetic branch different to that that leads to JA (de León et al. 2002). The differential impact of genes encoding oxylipin biosynthesis (α-*DOX1*) and JA perception (*COI1*) on virus synergism-associated cell death suggests an antagonistic relationship between products of α-DOX1 and the JA pathway. Functional diversification of JA and other oxylipins has been reported in signaling mechanisms that mediate root development and plant defenses in *Arabidopsis* (Velosillo et al. 2007).

In summary, our study demonstrates that SN induced by a PVX recombinant virus expressing the PPV HC-Pro was associated with PCD. Despite the SN response being clustered with the incompatible response by the similarity of their overall gene expression profiles, both hormone determination and clustering analyses of defense- or hormone-responsive genes suggest a role for proteasome in the SN associated with the compatible interaction. In addition, we also show that the jasmonate signaling pathway interferes with cell death caused by the PVX–*Potyvirus* synergistic interaction.

MATERIALS AND METHODS

Biological materials.

N. benthamiana plants were grown in a growth chamber with a cycle of 16 h of light and 8 h of darkness at 25°C. The infectious cDNA clones of PVX-HCWT and PVX-HCLH have been described previously (González-Jara et al. 2005). They were based on plasmid pP2C2S-402, a cDNA clone of PVX (strain UK-3) derived from pP2C2S (Baulcombe et al. 1995). PVX-HCWT contains a functional, translatable HC-Pro version from PPV, while PVX-HCLH contains a PPV HC-Pro version with a leucine to histidine mutation in amino acid 134 that makes it nonfunctional in suppression of gene silencing. Infectious RNA transcripts from TMV-GFP were obtained from TMV-GFP 1056, derived from TMV p30B.GFP with modifications in the virus movement protein gene (Lacomme and Santa Cruz 1999).

All plasmids were linearized with *Spe*I or *Kpn*I, and RNA transcripts were made by using T7 RNA polymerase as described (González-Jara et al. 2005). Transcript RNAs were inoculated onto leaves of *N. benthamiana*. The first leaves showing systemic symptoms were collected and ground in 10 volumes of 20 mM sodium phosphate buffer (pH 7.0). The extracts were clarified by centrifugation for 5 min at 5,000 × *g*, and the resulting supernatants were divided into aliquots and kept at –80°C. These crude virus preparations were used for the inoculation of *N. benthamiana* plants by applying 10 μl of sap inoculum onto Carborundum-dusted leaves.

The *N gene*-transgenic *N. benthamiana* line 310 A has been described previously (Peart et al. 2002). Infectious sap from TMV-GFP-infected plants was used to inoculate wild-type and *N*-transgenic *N. benthamiana* plants. Inoculated plants were maintained in a growth cabinet at 32°C with a 16-h photoperiod (80 $\mu Em^{-2}\ s^{-1}$) for 6 days before transfer to a growth chamber at 25°C to induce and synchronize the HR, which is induced on recognition of TMV-GFP.

RNA isolation and microarray analysis.

Per time and treatment, three independent biological replicates were used to monitor differences in gene expression between treatments. For each biological replicate, two symptomatic, noninoculated upper leaves from each of 10 plants per treatment were harvested and immediately frozen in liquid N_2. Total RNA was extracted from plant leaves using Trizol reagent (Invitrogen, San Diego, CA, U.S.A.), followed by purification with RNeasy midiprep columns (Qiagen, Hilden, Germany). RNA quantification and RNA quality determination were done as described (Adie et al. 2007). RNA was screened by Northern blot to ensure that recombinant PVX viruses retained the *HC-Pro* gene (Gonzalez-Jara et al. 2005).

The Agilent's 4-by-44 K Tobacco microarray contains 40,375 nonredundant probes (catalogue number G2519F-021113). Hybridization and scanning of slides was performed in accordance with the work of Adie and associates (2007). The statistical significance of the results was evaluated by the nonparametric algorithm Rank Products (Breitling et al. 2004) and available as RankProd package at Bioconductor (Hong et al. 2006). This method detects genes that are consistently highly ranked in several replicated experiments independently of their numerical intensities. The results are provided in the form of *P* values defined as the probability that a given gene is ranked in the observed position by chance. To control the FDR, *P* values were corrected using the method of Benjamani and Hochberg (1995). Genes with an FDR-corrected $P < 0.05$ and a fold-change of >1.5 or <0.67 were selected for further investigation. The expression profiles resulting from different treatments were clustered based on their similarity in expression using hierarchical complete linkage algorithm and Euclidean distance metric implemented in Cluster 3.0 (Eisen et al. 1998). The clustering results were visualized by a gene tree heat map using the TreeView program (Saldanha 2004). Clustering analysis was also performed with GEDI clustering software using default parameters (Eichler et al. 2003). The GEDI approach was used because, unlike "traditional" clustering algorithms, it captures in a two-dimensional diagram the complexity of the whole transcriptome.

Overrepresentation analysis.

Functional annotations for the probes represented in the microarray were taken from any of the following sources: i) the best BLASTX hit of *A. thaliana* proteins (*e* value $<1 \times 10^{-10}$), ii) the BLASTX hit of nonredundant proteins from GenBank using the program Blast2GO (Conesa et al. 2005), and iii) the available GO information for *N. tabacum* available on The Institute for Genomic Research website. In total, 20,367 (50.4%) of the probes that are monitored with the array were annotated by either method.

The enrichment analysis was created using a Cytoscape plugin called ClueGO (Bindea et al. 2009). GO analysis was carried out using a reference set based on GO annotations as described above. A right-sided hypergeometric test yielded the enrichment for GO terms within biological process category. Benjamini-Hochberg correction for multiple testing controlled the *P* values. ClueGO visualizes the selected terms in a functionally grouped annotation network that reflects the relationships between the terms based on the similarity of their associated genes. The degree of connectivity between terms is calculated using kappa statistics. A kappa score of 0.3 was used in this study. The calculated kappa score is also used for defining functional groups. The GO Term Grouping setting was on, with an initial group size of 2 and group merging set at 50%. The group leading term is the most significant term of the group. Multicolored networks contain GO terms shared by more than one functional group. The not-grouped terms are shown in white. The probes for which there was no GO annotation were not recognized in the test or reference set by ClueGO and, thus, they were not taken into account in the overrepresentation analysis. Only GO terms with corrected P values < 0.005 were considered to be overrepresented in our analysis.

TUNEL and cell death assays.

The TUNEL assay was performed using the In Situ cell death detection kit, fluorescein (Roche Diagnostics, Barcelona, Spain) according to the manufacturer's instructions. Before detection, systemically infected leaves were fixed, embedded in Paraplast, and sectioned in longitudinal sections. Sections (3 μm) were cut on glass slides, were dewaxed in xylene, were rehydrated, and were then pretreated with proteinase K at 20 μg/ml. Slides treated with DNaseI at 1,500 U/ml in 50 mM Tris-HCl (pH 7.5), 10 mM $MgCl_2$, and bovine serum albumin at 1 mg/ml for 10 min at room temperature served as positive controls. Consecutive slides were treated with 4′,6-diamidino-2-phenylindole for nuclei staining. For cell death analyses,

leaves were stained with lactophenol-trypan blue as described (Hamberg et al. 2003). Representative phenotypes were photographed with a Leica L2 stereoscope and Leica DM 2500 microscope using a Leica DFC 320 camera.

Cell damage was assayed by measuring electrolyte leakage as described by De León and associates (2002). Twenty-five disks of 0.3 cm^2 were excised from upper leaf tissue using a core borer. Disks were rinsed briefly with water and floated on 5 ml of double-distilled water for 6 h at room temperature. The conductivity of the water was measured using a Crinson conductivity meter. This represented the ion leakage from the leaf discs (reading 1). Then, samples were boiled for 20 min at 90°C. After the liquid cooled, the conductivity of the water was measured again. This represented the total ions present in the leaf discs (reading 2). Electrolyte leakage was represented as the percentage of total ions released (reading 1/reading 2 × 100). Reported data are means and standard errors of the values obtained in three independent experiments with pools from 5 to 10 plants for each treatment. Statistical analyses (analysis of variance followed by Duncan's multiple range test) were performed using the statistical software STATGRAPHICS Plus 5.1 (Statistical Graphics Corp, Englewood Cliffs, NJ, U.S.A.).

qRT-PCR and RT-PCR analyses.

qRT-PCR reactions were performed in the Rotor-Gene 6000 real-time PCR detection system (Corbett Research, Mortlake, Australia). One-step qRT-PCR was performed using total RNA preparations treated with TURBO DNA-free kit (Ambion, Austin, TX, U.S.A.). The real-time assay was performed using 15 µl of a reaction mix that contained 7.5 µl of Brilliant III Ultra-Fast qRT-PCR Master Mix (Agilent, Madrid), 1.8 µl of RNase-free water, 0.75 µl of reverse transcriptase, 0.15 µl of 100 mM dithiothreitol, 0.3 µM each primer, and 3 µl of total RNA extract (approximately 10 ng RNA/µl). qRT-PCR assays with and without reverse transcriptase were run in parallel, to ensure the absence of DNA template in the samples. All reactions were done in triplicate and the values obtained averaged. qRT-PCR was carried out at 50°C for 10 min, 95°C for 3 min, and 40 cycles of 95°C for 10 s and 60°C for 20 s. Synthesis of cDNA products of approximately 150 bp in length was confirmed by melting curve analysis using the Rotor-Gene 6000 software. 18S rRNAs were chosen for normalization because of their similar level of expression across all virus infections and their PCR amplification efficiencies.

RT-PCR for the analysis of *AOS*, *9-LOX*, *13-LOX*, and α-*DOX1* gene expression after methyl jasmonate (MeJA) treatment was performed as described by García-Marcos and associates (2009). The gene-specific oligonucleotides used to amplify partial cDNA fragments were the same used for qRT-PCR. The *Actin* gene transcripts were amplified as an internal control. A PCR using template derived from RNA without reverse transcription was performed as a negative control.

VIGS.

A 520-bp cDNA fragment of *PBE* from *N. benthamiana* was amplified by PCR using oligonucleotides PBE-F1 and PBE-R1. A 186-bp fragment of *NbCOI1* was amplified using oligonucleotides COI1-F1 and COI1-R1. The cDNA fragments were subsequently cut with *Bam*HI and *Xho*I and ligated into the binary vector pTRV2 to yield pTRV2:*NbPBE* and pTRV2:*NbCOI1*, respectively (Liu et al. 2004). The pTRV1 vector and the pTRV2 vector and its derivatives were separately transformed into *Agrobacterium tumefaciens* 2260. *N. benthamiana* leaves were infiltrated with *A. tumefaciens* cultures as described (Tenllado and Díaz-Ruíz 2001).

Total RNA was extracted from upper, noninoculated leaf tissue at different days after infiltration. Silencing of *NbPBE* and *NbCOI1* mRNAs were detected by qRT-PCR as described above. The following gene-specific primers that anneal outside the region targeted for silencing to ensure that the endogenous gene is tested were used: for *NbPBE* silencing, PBE-F2 and PBE-R2; for *NbCOI1* silencing,: COI1-F2 and COI1-R2.

MeJA and BTH treatments.

Four-week-old plants were treated with either 250 µM MeJA (Sigma) or mock solution (containing 250 µM ethanol) using foliar sprays. After spraying, plants were covered with a plastic cover and samples were harvested at 24 h. For BTH treatment, plants were sprayed with either 1 mM BTH or water solution (1.4% acetone and 0.02% Tween-20) for six consecutive days.

Hormone analysis.

Dry tissue (0.05 g) was homogenized in 2.5 ml of ultrapure water. A mixture of internal standards was added before the extraction (100 ng of $[^2H_6]$-ABA, 100 ng $[^2H_4]$-SA, and dihydrojasmonic acid). Extractions and experimental procedures were performed as described by Flors and associates (2008). After extraction, a 20-µl aliquot was directly injected into the high-performance liquid chromatography (HPLC) system. Analyses were carried out using a Waters Alliance 2690 HPLC system (Milford, MA, U.S.A.) with a nucleosil ODS reversed-phase column (100 by 2 mm i.d.; 5 µm) (Scharlab, Barcelona, Spain). The chromatographic system was interfaced to a Quatro LC (quadrupole-hexapolequadrupole) mass spectrometer (Micromass, Manchester, U.K.).

ACKNOWLEDGMENTS

R. Pacheco was the recipient of a contract from the Consejo Superior de Investigaciones Científicas (CSIC). A. García-Marcos was the recipient of a CSIC JAE-Doc contract from the program "Junta para la Ampliación de Estudios," co-funded by the European Social Funds. This work was supported by grant BIO2009-10172 from the Spanish Ministerio de Ciencia e Innovación. We thank the Servicio Central de Instrumentación Científica of the Universitat Jaume I, S. Chapman for providing the cDNA clone of TMV-GFP 1056, D. Baulcombe for providing the *N*-transgenic *N. benthamiana* (line 310 A), G. Bindea for advice in Cluego analysis, and T. Canto for critically reading the manuscript.

LITERATURE CITED

Adie, B. A., Pérez-Pérez, J., Pérez-Pérez, M. M., Godoy, M., Sánchez-Serrano, J. J., Schmelz, E. A., and Solano, R. 2007. ABA is an essential signal for plant resistance to pathogens affecting JA biosynthesis and the activation of defenses in *Arabidopsis*. Plant Cell 19:1665-1681.

Atsumi, G., Kagaya, U., Kitazawa, H., Nakahara, K. S., and Uyeda, I. 2009. Activation of the salicylic acid signaling pathway enhances *Clover yellow vein virus* virulence in susceptible pea cultivars. Mol. Plant-Microbe Interact. 22:166-175.

Ballut, L., Drucker, M., Pugnière, M., Cambon, F., Blanc, S., Roquet, F., Candresse, T., Schmid, H. P., Nicolas, P., Le Gall, O., and Badaoui, S. 2005. HcPro, a multifunctional protein encoded by a plant RNA virus, targets the 20S proteasome and affects its enzymic activities. J. Gen. Virol. 86:2595-2603.

Baulcombe, D. C., Chapman, S., and Santa-Cruz, S. 1995. Jellyfish green fluorescent protein as a reporter for virus infections. Plant J. 7:1045-1053.

Benjamani, Y., and Hochberg, Y. 1995. Controlling the false discovery rate: A practical and powerful approach to multiple testing. J. R. Stat. Soc. B (Ser. A) 57:289-300.

Bindea, G., Mlecnik, B., Hackl, H., Charoentong, P., Tosolini, M., Kirilovsky, A., Fridman, W. H., Pagès, F., Trajanoski, Z., and Galon, J. 2009. ClueGO: A Cytoscape plug-in to decipher functionally grouped gene ontology and pathway annotation networks. Bioinformatics 25:1091-1093.

Bolton, M. D. 2009. Primary metabolism and plant defense: Fuel for the fire. Mol. Plant-Microbe Interact. 22:487-497.

Breitling, R., Armengaud, P., Amtmann, A., and Herzyk, P. 2004. Rank

products: A simple, yet powerful, new method to detect differentially regulated genes in replicated microarray experiments. FEBS (Fed. Eur. Biochem. Soc.) Lett. 573:83-92.
Burgyán, J., Hornyik, C., Szittya, G., Silhavy, D., and Bisztray, G. 2000. The ORF1 products of tombusviruses play a crucial role in lethal necrosis of virus-infected plants. J. Virol. 74:10873-10881.
Chini, A., Boter, M., and Solano, R. 2009. Plant oxylipins: COI1/JAZs/MYC2 as the core jasmonic acid-signalling module. FEBS (Fed. Eur. Biochem. Soc.) J. 276:4682-4692.
Conesa, A., Gotz, S., García-Gomez, J. M., Terol, J., Talón, M., and Robles, M. 2005. Blast2GO: A universal tool for annotation, visualization and analysis in functional genomics research. Bioinformatics 21:3674-3676.
Cosgrove, D. J. 2005. Growth of the plant cell wall. Nat. Rev. Mol. Cell Biol. 6:850-861.
Craig, A., Ewan, R., Mesmar, J., Gudipati, V., and Sadanandom, A. 2009. E3 ubiquitin ligases and plant innate immunity. J. Exp. Bot. 60:1123-1132.
Dangl, J. L., and Jones, J. D. 2001. Plant pathogens and integrated defence responses to infection. Nature 411:826-833.
De León, I. P.Sanz, A., Hamberg, M., and Castresana, C. 2002. Involvement of the *Arabidopsis* α-DOX1 fatty acid dioxygenase in protection against oxidative stress and cell death. Plant J. 29:61-72.
Dielen, A. S., Badaoui, S., Candresse, T., and German-Retana, S. 2010. The ubiquitin/26S proteasome system in plant–pathogen interactions: A never-ending hide-and-seek game. Mol. Plant Pathol. 11:293-308.
Dielen, A. S., Sassaki, F. T., Walter, J., Michon, T., Ménard, G., Pagny, G., Krause-Sakate, R., Maia, I.de G., Badaoui, S., Le Gall, O., Candresse, T., and German-Retana, S. 2011. The 20S proteasome α5 subunit of *Arabidopsis thaliana* carries an RNase activity and interacts in planta with the lettuce mosaic potyvirus HcPro protein. Mol. Plant Pathol. 12:137-50.
Dinesh-Kumar, S. P., Tham, W. H., and Baker, B. J. 2000. Structure-function analysis of the *Tobacco mosaic virus* resistance gene *N*. Proc. Natl. Acad. Sci. U.S.A. 97:14789-14794.
Eichler, G. S., Huang, S., and Ingber, D. E. 2003. Gene Expression Dynamics Inspector (GEDI): For integrative analysis of expression profiles. Bioinformatics 19:2321-2322.
Eisen, M. B., Spellman, P. T., Brown, P. O., and Botstein, D. 1998. Cluster analysis and display of genome-wide expression patterns. Proc. Natl Acad. Sci. U.S.A. 95:14863-14868.
Flors, V., Ton, J., van Doorn, R., Jakab, G., García-Agustín, P., and Mauch-Mani, B. 2008. Interplay between JA, SA and ABA signalling during basal and induced resistance against *Pseudomonas syringae* and *Alternaria brassicicola*. Plant J. 4:81-92.
Friedrich, L., Lawton, K., Ruess, W., Masner, P., Specker, N., Rella, M. G., Meier, B., Dincher, S., Staub, T., Uknes, S., Métraux, JP., Kessmann, H., and Ryals, J. 1996. A benzothiadiazole derivative induces systemic acquired resistance in tobacco. Plant J. 10:61-70.
Garcia-Marcos, A., Pacheco, R., Martiáñez, J., González-Jara, P., Díaz-Ruíz, J. R., and Tenllado, F. 2009. Transcriptional changes and oxidative stress associated with the synergistic interaction between *Potato virus X* and *Potato virus Y* and their relationship with symptom expression. Mol. Plant-Microbe Interact. 22:1431-1444.
Gavrieli, Y., Sherman, Y., and Ben-Sasson, S. A. 1992. Identification of programmed cell death in situ via specific labeling of nuclear DNA fragmentation. J. Cell Biol. 119:493-501.
González-Jara, P., Atencio, F. A., Martínez-García, B., Barajas, D., Tenllado, F., and Díaz-Ruíz, J. R. 2005. A single amino acid mutation in the *Plum pox virus* helper component-proteinase gene abolishes both synergistic and RNA silencing suppression activities. Phytopathology 95:894-901.
Hamberg, M., Sanz, A., Rodriguez, M. J., Calvo A. P., and Castresana, C. 2003. Activation of the fatty acid α-dioxygenase pathway during bacterial infection of tobacco leaves. Formation of oxylipins protecting against cell death. J. Biol. Chem. 278:51796-51805.
Hammond-Kosack, K. E., and Jones, J. D. 1996. Resistance gene-dependent plant defense responses. Plant Cell 8:1773-1791.
Hatsugai, N., Iwasaki, S., Tamura, K., Kondo, M., Fuji, K., Ogasawara, K., Nishimura, M., and Hara-Nishimura, I. 2009. A novel membrane fusion-mediated plant immunity against bacterial pathogens. Genes Dev. 23:2496-2506.
Hoeberichts, F. A., and Woltering, E. J. 2003. Multiple mediators of plant programmed cell death: Interplay of conserved cell death mechanisms and plant-specific regulators. Bioessays. 25:47-57.
Hong, F., Breitling, R., McEntee, C. W., Wittner, B. S., Nemhauser, J. L., and Chory, J. 2006. RankProd: A bioconductor package for detecting differentially expressed genes in meta-analysis. Bioinformatics 22:2825-2827.
Huang, Z., Yeakley, J. M., Garcia, E. W., Holdridge, J. D., Fan, J. B., and Whitham, S. A. 2005. Salicylic acid-dependent expression of host genes in compatible *Arabidopsis*–virus interactions. Plant Physiol. 137:1147-1159.
Jones, J. D. G., and Dangl, J. L. 2006. The plant immune system. Nature 444:323-329.
Kasschau, K. D., Xie, Z., Allen, E., Llave, C., Chapman, E. J., Krizan, K. A., and Carrington. J. C. 2003. P1/HC-Pro, a viral suppressor of RNA silencing, interferes with *Arabidopsis* development and miRNA function. Dev. Cell. 4:205-217.
Kim, B., Masuta, C., Matsuura, H., Takahashi, H., and Inukai, T. 2008. Veinal necrosis induced by *Turnip mosaic virus* infection in *Arabidopsis* is a form of defense response accompanying HR-like cell death. Mol. Plant-Microbe Interact. 21:260-268.
Kim, B. M., Suehiro, N., Natsuaki, T., Inukai, T., and Masuta, C. 2010. The P3 protein of *Turnip mosaic virus* can alone induce hypersensitive response-like cell death in *Arabidopsis thaliana* carrying *TuNI*. Mol. Plant-Microbe Interact. 23:144-152.
Kim, M., Ahn, J. W., Jin, U. H., Choi, D., Paek, K. H., and Pai, H. S. 2003. Activation of the programmed cell death pathway by inhibition of proteasome function in plants. J Biol. Chem. 278:19406-19415.
Király, L., Cole, A. B., Bourque, J. E., and Schoelz, J. E. 1999. Systemic cell death is elicited by the interaction of a single gene in *Nicotiana clevelandii* and gene VI of *Cauliflower mosaic virus*. Mol. Plant-Microbe Interact. 12:919-925.
Komatsu, K., Hashimoto, M., Ozeki, J., Yamaji, Y., Maejima, K., Senshu, H., Himeno, M., Okano, Y., Kagiwada, S., and Namba, S. 2010. Viral-induced systemic necrosis in plants involves both programmed cell death and the inhibition of viral multiplication, which are regulated by independent pathways. Mol. Plant-Microbe Interact. 23:283-293.
Komatsu, K., Hashimoto, M., Maejima, K., Shiraishi, T., Neriya, Y., Miura, C., Minato, N., Okano, Y., Sugawara, K., Yamaji, Y., and Namba, S. 2011. A necrosis-inducing elicitor domain encoded by both symptomatic and asymptomatic *Plantago asiatica mosaic virus* isolates, whose expression is modulated by virus replication. Mol. Plant-Microbe Interact. 24:408-420.
Kunkel, B. N., and Brooks, D. M. 2002. Cross talk between signalling pathways in pathogen defense. Curr. Opin. Plant Biol. 5:325-331.
Lacomme, C., and Santa Cruz, S. 1999. Bax-induced cell death in tobacco is similar to the hypersensitive response. Proc. Natl. Acad. Sci. U.S.A. 96:7956-7961.
Lamb, C., and Dixon, R. A. 1997. The oxidative burst in plant disease resistance. Annu. Rev. Plant Physiol. Plant Mol. Biol. 48:251-275.
Lewsey, M., Palukaitis, P., and Carr, J. P. 2009. Plant–virus interactions: Defence and counter-defence. Pages 134-176 in: Molecular Aspects of Plant Disease Resistance. J. Parker, ed. Wiley-Blackwell, Oxford.
Liu, Y., Schiff, M., and Dinesh-Kumar, S. P. 2004. Involvement of MEK1 MAPKK, NTF6 MAPK, WRKY/MYB transcription factors, *COI1* and *CTR1* in *N*-mediated resistance to *Tobacco mosaic virus*. Plant J. 38:800-809.
Liu, Y., Ren, D., Pike, S., Pallardy, S., Gassmann, W., and Zhang, S. 2007. Chloroplast-generated reactive oxygen species are involved in hypersensitive response-like cell death mediated by a mitogen-activated protein kinase cascade. Plant J. 51:941-954.
Lundgren, J., Masson, P., Realini, C. A., and Young, P. 2003. Use of RNA interference and complementation to study the function of the *Drosophila* and human 26S proteasome subunit S13. Mol. Cell Biol. 23:5320-5330.
Maere, S., Heymans, K., and Kuiper, M. 2005. *BiNGO*: A Cytoscape plugin to assess overrepresentation of Gene Ontology categories in biological networks. Bioinformatics 21:3448-3449.
Peart, J. R., Cook, G., Feys, B. J., Parker, J. E., and Baulcombe, D. C. 2002. An *EDS1* orthologue is required for *N*-mediated resistance against *Tobacco mosaic virus*. Plant J. 29:569-579.
Pruss, G., Ge, X., Shi, X. M., Carrington, J. C., and Vance, V. B. 1997. Plant viral synergism: The potyviral genome encodes a broad-range pathogenicity enhancer that transactivates replication of heterologous viruses. Plant Cell 9:859-868.
Saldanha, A. J. 2004. Java Treeview—extensible visualization of microarray data. Bioinformatics 20:3246-3248.
Seo, Y. S., Rojas, M. R., Lee, J. Y., Lee, S. W., Jeon, J. S., Ronald, P., Lucas, W. J., and Gilbertson, R. L. 2006. A viral resistance gene from common bean functions across plant families and is up-regulated in a non-virus-specific manner. Proc. Natl. Acad. Sci. U.S.A. 103:11856-11861.
Shimizu, T., Satoh, K., Kikuchi, S., and Omura, T. 2007. The repression of cell wall- and plastid-related genes and the induction of defense-related genes in rice plants infected with *Rice dwarf virus*. Mol. Plant-Microbe Interact. 20:247-254.
Soitamo, A. J., Jada, B., and Lehto, K. 2011. HC-Pro silencing suppressor significantly alters the gene expression profile in tobacco leaves and

flowers. BMC Plant Biol. 11:68-83.
Tao, Y., Xie, Z., Chen, W., Glazebrook, J., Chang, H. S., Han, B., Zhu, T., Zou, G., and Katagiri, F. 2003. Quantitative nature of *Arabidopsis* responses during compatible and incompatible interactions with the bacterial pathogen *Pseudomonas syringae*. Plant Cell 15:317-330.
Tenllado, F., and Díaz-Ruíz, J. R. 2001. Double-stranded RNA-mediated interference with plant virus infection. J. Virol. 75:12288-12297.
Vellosillo, T., Martínez, M., López, M. A., Vicente, J., Cascón, T., Dolan, L., Hamberg, M., and Castresana, C. 2007. Oxylipins produced by the 9-lipoxygenase pathway in *Arabidopsis* regulate lateral root development and defense responses through a specific signaling cascade. Plant Cell 19:831-846.
Whitham, S. A., Yang, C., and Goodin, M. 2006. Global impact: Elucidating plant responses to viral infection. Mol. Plant-Microbe Interact. 19:1207-1215.
Xu, P., and Roossinck, M. J. 2000. *Cucumber mosaic virus* D satellite RNA-induced programmed cell death in tomato. Plant Cell 12:1079-1092.
Yang, C., Guo, R., Jie, F., Nettleton, D., Peng, J., Carr, T., Yeakley, J. M., Fan, J. B., and Whitham, S. A. 2007. Spatial analysis of *Arabidopsis thaliana* gene expression in response to *Turnip mosaic virus* infection. Mol. Plant-Microbe Interact. 20:358-370.

AUTHOR-RECOMMENDED INTERNET RESOURCES

Gene expression dynamics inspector (GEDI) clustering software:
web1.tch.harvard.edu/research/ingber/GEDI/gedihome.htm
ClueGO Gene Ontology tool:
www.ici.upmc.fr/cluego/cluegoDownload.shtml